Dossier

This paper is a part of the hereunder thematic dossier published in OGST Journal, Vol. 69, No. 4, pp. 507-766 and available online here

Cet article fait partie du dossier thématique ci-dessous publié dans la revue OGST, Vol. 69, n°4 pp. 507-766 et téléchargeable ici

---

DOSSIER Edited by/Sous la direction de : **Z. Benjelloun-Touimi**

Geosciences Numerical Methods
Modélisation numérique en géosciences

ifp *Energies nouvelles*

Modeling Fractures in a Poro-Elastic Medium

Benjamin Ganis[1], Vivette Girault[2,3]*, Mark Mear[1], Gurpreet Singh[1] and Mary Wheeler[1]

[1] Center for Subsurface Modeling, Institute for Computational Engineering and Sciences, The University of Texas at Austin, Austin, TX 78712 - USA
[2] Laboratoire Jacques-Louis Lions, UPMC, Université Paris 6, 4 place Jussieu, 75005 Paris - France
[3] Department of Mathematics, TAMU, College Station, TX 77843 - USA
e-mail: bganis@ices.utexas.edu - girault@ann.jussieu.fr - mear@mail.utexas.edu - gurpreet@ices.utexas.edu - mfw@ices.utexas.edu

* Corresponding author

Résumé — **Un modèle de fracture dans un milieu poro-élastique** — Nous présentons un modèle de fracture dans un milieu poro-élastique. Il décrit la fracture comme une courbe ou une surface, selon la dimension, l'épaisseur étant incorporée dans l'équation de l'écoulement dans la fracture. La discrétisation utilise des éléments finis mixtes pour le fluide et des éléments finis continus pour le déplacement du milieu. Le schéma est résolu par un algorithme qui découple, d'une part, le calcul du déplacement de celui de l'écoulement, et d'autre part, le calcul de l'écoulement dans le réservoir de celui dans la fracture. Le modèle est illustré par un essai numérique.

Abstract — *Modeling Fractures in a Poro-Elastic Medium* — *We present a fracture model in a poro-elastic medium. The model describes the fracture as a curve or surface according to the dimension, the width of the crack being included into the equation of flow in the fracture. The discretization uses mixed finite elements for the fluid and continuous finite elements for the porous medium's displacement. The numerical scheme is solved by an algorithm that decouples, on one hand, the computation of the mechanics from that of the fluid, and on the other hand, the computation of the flow in the reservoir from that in the fracture. The model is illustrated by a numerical experiment.*

INTRODUCTION

In petroleum and environmental engineering, studies of multiscale and multiphysics phenomena such as reservoir deformation, surface subsidence, well stability, sand production, waste deposition, hydraulic fracturing, and CO_2 sequestration [1] require a clear understanding of both the fluid flow and solid phase mechanical response.

Traditionally, fluid flow problems were focused on reservoir flow whereas the influence of porous media deformation on pore pressure was usually simplified and approximated as a constant rock compressibility that could not account for rock response especially in naturally fractured and/or stress-sensitive reservoirs [2]. In this setting, models for narrow fractures can be derived by treating the width as a small parameter ε and letting this parameter tend to zero. One approach in this direction can be found in the theoretical analysis of Morales and Showalter [3, 4], where only flow is considered, the crack has a flat basis and vertical height of the order of ε, and the pressure is continuous at the interfaces. The former reference deals with the divergence form of Darcy's law and the latter with the mixed form. Another approach consists in treating the fracture as a thin domain in the framework of domain decomposition. We refer the reader to the extensive work of Alboin *et al.* [5] and Martin *et al.* [6] on Darcy flow.

To overcome the limitations of decoupled flow simulation, solving the coupled fluid flow and mechanics model in porous media setting has become more feasible with emerging computational machine power.

In 1941, Biot [7] proposed the first three-dimensional consolidation theory. Later, poro-elasticity and poro-plasticity models for single phase, black oil, and compositional flow models were developed following Biot's work [2, 8-12].

There are three approaches that are currently employed in the numerical coupling of fluid flow and the mechanical response of the reservoir solid structure [9, 12]. They have been referred to in the literature as fully implicit, loose or explicit coupling, and iterative coupling. The fully implicit involves solving all of the governing equations simultaneously and involves careful implementation with substantial local memory and complex solvers. The loosely or explicitly coupled is less accurate and requires estimates of when to update the mechanic response. Iterative coupling is a sequential procedure where either the flow or the mechanics is solved first, followed by incorporating the latest solution information. At each step, the procedure is iterated until the solution converges within an acceptable tolerance. This last approach appears to be more scalable on emerging exascale computer platforms; it can also be used as a preconditioner for the fully implicit coupling. But of course, iterative coupling schemes must be carefully designed. For instance, two iterative coupling schemes, the undrained split and the fixed stress split, are of particular interest; they converge for slightly compressible linearized flow [13]. In contrast, a Von Neumann stability analysis shows that the drained split and the fixed strain split iterative methods are not stable for the same model problem [9].

Hydraulic fracking is one of the primary ways manufacturers retrieve natural gas. Hence, modeling fractures in porous media, that are either naturally present or are created by stimulation processes, is a high profile topic, but it is also a source of additional and challenging complexities. This work focuses on the simulation of the time-dependent flow of a fluid in a deformable porous medium that contains a crack. The medium in which the crack is embedded is governed by the standard equations of linear poro-elasticity and the flow of the fluid within the crack is governed by a specific channel flow relation. The two key assumptions of this channel flow equation are:

– the width of the crack is small compared to its other relevant dimensions, and is such that the crack can be represented as a single surface. The relevant kinematical data is the jump in the displacement of the medium across the crack, *i.e.* the crack's width;
– the permeability in the crack is much larger than in the reservoir.

One advantage of treating the crack as a single surface is that it alleviates the need for meshing a thin region, thus avoiding all the complexities related to anisotropic elements.

In this paper, we formulate a discretization that is suitable for irregular and rough grids and discontinuous full tensor permeabilities that are often encountered in modeling subsurface flows. To this end, we develop a multiphysics algorithm that couples Multipoint Flux Mixed Finite Element (MFMFE) methods for the fluid, both in the medium and in the crack, with continuous Galerkin finite element methods (CG) for the elastic displacement. The MFMFE method was developed for Darcy flow in [14-16]. It is locally conservative with continuous fluxes and can be viewed within a variational framework as a mixed finite element method with special approximating spaces and quadrature rules. It allows for an accurate and efficient treatment of irregular geometries and heterogeneities such as faults, layers, and pinchouts that require highly distorted grids and discontinuous coefficients. The resulting discretizations are cell-centered with convergent pressures and velocities on general hexahedral and simplicial grids. The MFMFE method is extended to poro-elasticity

in [17]; the analysis is based on the technique developed by Phillips and Wheeler in [18].

We solve the numerical scheme by an extension to discrete fractures of the fixed stress splitting algorithm. Its salient features at each time step are:
– we decouple the computation of the displacement from that of the fluid flow until convergence;
– we decouple the computation of the fluid flow in the reservoir from that of the flow in the crack until convergence.

The model described here does not include crack propagation, *i.e.* the crack front is stationary. However, the work presented here can be viewed as a starting point toward hydraulic fracture modeling in which non planar crack propagation is simulated. Our future plans include coupling the present software with the HYFRAC boundary element method developed by Mear and discussed in [19], as well as treating multiple cracks or multiphase flow in the reservoir and non Newtonian flow in the fracture.

This article is organized as follows. The modeling equations are defined in Section 1. Section 2 summarizes theoretical results on the linear model. The numerical scheme and algorithm are described in Section 3. A numerical experiment illustrating the model is presented in Section 4. We end with some conclusions.

1 PROBLEM FORMULATION

Let the reservoir Ω be a bounded domain of R^d $d = 2$ or 3, with piecewise smooth Lipschitz boundary $\partial\Omega$ and exterior normal $\boldsymbol{n}$. Let the fracture $\mathscr{C} \Subset \Omega$ be a simple piecewise smooth curve with endpoints $\boldsymbol{a}$ and $\boldsymbol{b}$ when $d = 2$ or a simple piecewise smooth surface with piecewise smooth Lipschitz boundary $\partial\mathscr{C}$ when $d = 3$. To simplify, we denote partial derivatives with respect to time by the index t.

1.1 Equations in $\Omega\backslash\mathscr{C}$

The displacement of the solid is modeled in $\Omega\backslash\mathscr{C}$ by the quasi-static Biot equations for a linear elastic, homogeneous, isotropic, porous solid saturated with a slightly compressible viscous fluid. The constitutive equation for the Cauchy stress tensor $\boldsymbol{\sigma}^{por}$ is:

$$\boldsymbol{\sigma}^{por}(\boldsymbol{u}, p) = \boldsymbol{\sigma}(\boldsymbol{u}) - \alpha p \boldsymbol{I} \qquad (1.1)$$

where $\boldsymbol{I}$ is the identity tensor, $\boldsymbol{u}$ is the solid's displacement, p is the fluid pressure, $\boldsymbol{\sigma}$ is the effective linear elastic stress tensor:

$$\boldsymbol{\sigma}(\boldsymbol{u}) = \lambda(\nabla \cdot \boldsymbol{u})\boldsymbol{I} + 2\,G\boldsymbol{\varepsilon}(\boldsymbol{u}) \qquad (1.2)$$

Here, $\lambda > 0$ and $G > 0$ are the Lamé constants, $\alpha > 0$ is the dimensionless Biot coefficient, and $\boldsymbol{\varepsilon}(\boldsymbol{u}) = (\nabla\boldsymbol{u} + \nabla\boldsymbol{u}^T)/2$ is the strain tensor. Then the balance of linear momentum in the solid reads:

$$-\nabla \cdot \boldsymbol{\sigma}^{por}(\boldsymbol{u}, p) = \boldsymbol{f} \ \text{ in } \Omega\backslash\mathscr{C} \qquad (1.3)$$

where $\boldsymbol{f}$ is a body force. For the fluid, we use a linearized slightly compressible single-phase model. Let p_r be a reference pressure, $\rho_f > 0$ the fluid phase density, $\rho_{f,r} > 0$ a constant reference density relative to p_r, and c_f the fluid compressibility. We consider the simplified case when ρ_f is a linear function of pressure:

$$\rho_f = \rho_{f,r}\big(1 + c_f(p - p_r)\big) \qquad (1.4)$$

Next, let φ^* denote the fluid content of the medium; it is related to the displacement and pressure by:

$$\varphi^* = \varphi_0 + \alpha\nabla \cdot \boldsymbol{u} + \frac{1}{M}p \qquad (1.5)$$

where φ_0 is the initial porosity, and M a Biot constant. The velocity of the fluid $\boldsymbol{v}^D$ in $\Omega\backslash\mathscr{C}$ obeys Darcy's Law:

$$\boldsymbol{v}^D = -\frac{1}{\mu_f}\boldsymbol{K}\big(\nabla p - \rho_f g\nabla\eta\big) \qquad (1.6)$$

where $\boldsymbol{K}$ is the absolute permeability tensor, assumed to be symmetric, bounded, uniformly positive definite in space and constant in time, $\mu_f > 0$ is the constant fluid viscosity, g is the gravitation constant, and η is the distance in the vertical direction, variable in space, but constant in time. The fluid mass balance in $\Omega\backslash\mathscr{C}$ reads:

$$(\rho_f\varphi^*)_t + \nabla \cdot (\rho_f\boldsymbol{v}^D) = q \qquad (1.7)$$

where q is a mass source or sink term taking into account injection into or out of the reservoir. The equation obtained by substituting (1.4) and (1.5) into (1.7) is linearized through the following considerations. The fluid compressibility c_f is of the order of 10^{-5} or 10^{-6}, *i.e.* it is small. The fraction p/M is small and the divergence of $\boldsymbol{u}$ is also small. Therefore these terms can be neglected. With these approximations, when dividing (1.7) by $\rho_{f,r}$, substituting (1.6), and setting $\tilde{q} = q/\rho_{f,r}$, we obtain:

$$\left(\frac{1}{M} + c_f\varphi_0\right)p_t + \alpha\nabla \cdot \boldsymbol{u}_t$$
$$-\nabla \cdot \left(\frac{1}{\mu_f}\boldsymbol{K}(\nabla p - \rho_{f,r}g\nabla\eta)\right) = \tilde{q} \qquad (1.8)$$

Thus the poro-elastic system we are considering for modeling the displacement $\boldsymbol{u}$ and pressure p in $\Omega\backslash\mathscr{C}$ is governed by (1.1), (1.3) and (1.8).

1.2 Equation in $\mathscr{C}$

The trace of p on $\mathscr{C}$ is denoted by p_c and $\overline{\nabla}$ is the surface gradient operator on $\mathscr{C}$, it is the tangential trace of the gradient. These quantities are well defined for our problem. The width of the fracture is represented by a non-negative function w defined on $\mathscr{C}$; it is the jump of the displacement $\boldsymbol{u}$ in the normal direction. Since the medium is elastic and the energy is finite, w must be bounded and must vanish on the boundary of the fracture. We adopt a channel flow relation for the crack in which the volumetric flow rate $\mathscr{Q}$ on $\mathscr{C}$ satisfies [1]:

$$\mathscr{Q} = -\frac{w^3}{12\mu_f}\left(\overline{\nabla} p_c - \rho_f g\overline{\nabla}\eta\right)$$

and the conservation of mass in the fracture satisfies:

$$(\rho_f w)_t = -\overline{\nabla}\cdot(\rho_f\mathscr{Q}) + q_I - q_L$$

Here, q_I is a known injection term into the fracture, and q_L is an unknown leakoff term from the fracture into the reservoir that guarantees the conservation of mass in the system. Approximating ρ_f by $\rho_{f,r}$ in the time derivative, linearizing the diffusion term as in the previous section, dividing by $\rho_{f,r}$, and setting $\tilde{q}_I = \frac{q_I}{\rho_{f,r}}$, $\tilde{q}_L = \frac{q_L}{\rho_{f,r}}$, yield the equation in $\mathscr{C}$:

$$w_t - \overline{\nabla}\cdot\left(\frac{w^3}{12\mu_f}\left(\overline{\nabla} p_c - \rho_{f,r} g\overline{\nabla}\eta\right)\right) = \tilde{q}_I - \tilde{q}_L \quad (1.9)$$

In order to specify the relation between the displacement $\boldsymbol{u}$ of the medium and the width w of the fracture, let us distinguish the two sides (or faces) of $\mathscr{C}$ by the superscripts $+$ and $-$; a specific choice must be selected but is arbitrary. To simplify the discussion, we use a superscript $\star$ to denote either $+$ or $-$. Let $\Omega^\star$ denote the part of Ω adjacent to $\mathscr{C}^\star$ and let $\boldsymbol{n}^\star$ denote the unit normal vector to $\mathscr{C}$ exterior to $\Omega^\star$, $\star = +, -$. As the fracture is represented geometrically by a figure with no width, then $\boldsymbol{n}^- = -\boldsymbol{n}^+$. For any function g defined in $\Omega\backslash\mathscr{C}$ that has a trace, let $g^\star$ denote the trace of g on $\mathscr{C}^\star$, $\star = +, -$. Then we define the jump of g on $\mathscr{C}$ in the direction of $\boldsymbol{n}^+$ by:

$$[g]_\mathscr{C} = g^+ - g^-$$

The width w is the jump of $\boldsymbol{u}\cdot\boldsymbol{n}^-$ on $\mathscr{C}$:

$$w = -[\boldsymbol{u}]_\mathscr{C}\cdot\boldsymbol{n}^+$$

Therefore the only unknown in (1.9) is the leakoff term $\tilde{q}_L$.

Summarizing, the equations in $\Omega\backslash\mathscr{C}$ are (1.3) and (1.8), and the equation in $\mathscr{C}$ is (1.9); the corresponding unknowns are $\boldsymbol{u}$, p and $\tilde{q}_L$. These equations are complemented in the next section by interface, boundary and initial conditions.

1.3 Interface, Boundary, and Initial Conditions

The balance of the normal traction vector and the conservation of mass yield the interface conditions on each side (or face) of $\mathscr{C}$:

$$(\boldsymbol{\sigma}^{\text{por}}(\boldsymbol{u},p))^\star\boldsymbol{n}^\star = -p_c\boldsymbol{n}^\star, \quad \star = +, - \quad (1.10)$$

Then the continuity of p_c through $\mathscr{C}$ yields:

$$[\boldsymbol{\sigma}^{\text{por}}(\boldsymbol{u},p)]_\mathscr{C}\boldsymbol{n}^+ = 0$$

The conservation of mass at the interface gives:

$$\frac{1}{\mu_f}[\boldsymbol{K}(\nabla p - \rho_{f,r}g\nabla\eta)]_\mathscr{C}\cdot\boldsymbol{n}^+ = \tilde{q}_L \quad (1.11)$$

General conditions on the exterior boundary $\partial\Omega$ of Ω can be prescribed for the poro-elastic system, but to simplify, we assume that the displacement $\boldsymbol{u}$ vanishes as well as the flux $\boldsymbol{K}(\nabla p - \rho_{f,r}g\nabla\eta)\cdot\boldsymbol{n}$. According to the above hypotheses on the energy and medium, we assume that w is bounded in $\mathscr{C}$ and vanishes on $\partial\mathscr{C}$. Finally, the only initial data that we need are the initial pressure and initial porosity, p_0 and φ_0. Therefore the complete problem statement, called Problem (Q), is: Find $\boldsymbol{u}$, p, and $\tilde{q}_L$ satisfying (1.1), (1.3), (1.8) in $\Omega\backslash\mathscr{C}$ and (1.9) in $\mathscr{C}$, for all time $t \in]0, T[$, with the interface conditions (1.10) and (1.11) on $\mathscr{C}$:

$$-\nabla\cdot\boldsymbol{\sigma}^{\text{por}}(\boldsymbol{u},p) = \boldsymbol{f}$$

$$\boldsymbol{\sigma}^{\text{por}}(\boldsymbol{u},p) = \boldsymbol{\sigma}(\boldsymbol{u}) - \alpha p\boldsymbol{I}$$

$$\left(\frac{1}{M} + c_f\varphi_0\right)p_t + \alpha\nabla\cdot\boldsymbol{u}_t$$
$$-\nabla\cdot\left(\frac{1}{\mu_f}\boldsymbol{K}(\nabla p - \rho_{f,r}g\nabla\eta)\right) = \tilde{q}$$

$$w_t - \overline{\nabla}\cdot\left(\frac{w^3}{12\mu_f}\left(\overline{\nabla} p_c - \rho_{f,r}g\overline{\nabla}\eta\right)\right) = \tilde{q}_I - \tilde{q}_L$$

$$(\boldsymbol{\sigma}^{\text{por}}(\boldsymbol{u},p))^\star\boldsymbol{n}^\star = -p_c\boldsymbol{n}^\star, \quad \star = +, - \text{ on } \mathscr{C}$$

$$\frac{1}{\mu_f}[\boldsymbol{K}(\nabla p - \rho_{f,r}g\nabla\eta)]_\mathscr{C}\cdot\boldsymbol{n}^+ = \tilde{q}_L \text{ on } \mathscr{C}$$

where $p_c = p_{|\mathscr{C}}$ and:

$$w = -[\boldsymbol{u}]_\mathscr{C}\cdot\boldsymbol{n}^+ \tag{1.12}$$

with the boundary conditions:

$$\boldsymbol{u} = 0, \, \boldsymbol{K}(\nabla p - \rho_{f,r}g\nabla\eta)\cdot\boldsymbol{n} = 0 \text{ on } \partial\Omega \tag{1.13}$$

$$w = 0 \text{ on } \partial\mathscr{C} \tag{1.14}$$

and the initial condition at time $t = 0$:

$$p(0) = p_0$$

2 THEORETICAL RESULTS

Problem (Q) is highly non linear and its analysis is outside the scope of this work. Therefore we present here some theoretical results on a linearized problem where (1.12) is substituted into the first term of (1.9) while the factor w^3 in the second term is assumed to be known. Knowing w^3 amounts to linearizing the nonlinear term with respect to w, such as could be encountered in a time-stepping algorithm.

2.1 Variational Formulation

It is convenient (but not fundamental) to generalize the notation of Section 1.2 by introducing an auxiliary partition of Ω into two non-overlapping subdomains Ω^+ and Ω^- with Lipschitz interface Γ containing $\mathscr{C}$, $\Omega^\star$ being adjacent to $\mathscr{C}^\star$, $\star = +, -$. The precise shape of Γ is not important as long as Ω^+ and Ω^- are both Lipschitz. Let $\Gamma^\star = \partial\Omega^\star\backslash\Gamma$; for any funtion g defined in Ω, we set $g^\star = g_{|\Omega^\star}$, $\star = +, -$. Let $W = H^1(\Omega^+ \cup \Omega^-)$, *i.e.*:

$$W = \{v \in L^2(\Omega); v^\star \in H^1(\Omega^\star), \star = +, -\}$$

normed by the graph norm:

$$||v||_W = (||v^+||^2_{H^1(\Omega^+)} + ||v^-||^2_{H^1(\Omega^-)})^{1/2}$$

The space for the displacement is:

$$V = \{v \in W^d; [v]_{\Gamma\backslash\mathscr{C}} = 0, v^\star_{|\Gamma^\star} = 0, \star = +, -\} \tag{2.1}$$

with the norm of W^d:

$$||v||_V = \left(\sum_{i=1}^d ||v_i||^2_W\right)^{\frac{1}{2}} \tag{2.2}$$

The space for the pressure is more subtle: it is H^1 in Ω, but in $\mathscr{C}$, it is:

$$H^1_w(\mathscr{C}) = \{z \in H^{1/2}(\mathscr{C}); w^{3/2}\overline{\nabla} z \in L^2(\mathscr{C})^{d-1}\} \tag{2.3}$$

equipped with the norm:

$$||z||_{H^1_w(\mathscr{C})} = (||z||^2_{H^{1/2}(\mathscr{C})} + ||w^{3/2}\overline{\nabla} z||^2_{L^2(\mathscr{C})})^{1/2} \tag{2.4}$$

where $H^{1/2}(\mathscr{C})$ is the space of traces on $\mathscr{C}$ of $H^1(\Omega)$ functions. Thus p belongs to the space:

$$Q = \{q \in H^1(\Omega); q_c \in H^1_w(\mathscr{C})\}, \, q_c := q|_\mathscr{C} \tag{2.5}$$

equipped with the graph norm:

$$||q||_Q = (||q||^2_{H^1(\Omega)} + ||q_c||^2_{H^1_w(\mathscr{C})})^{1/2} \tag{2.6}$$

Finally, the space for the leakoff variable $\tilde{q}_L$ is $H^1_w(\mathscr{C})'$, the dual space of $H^1_w(\mathscr{C})$, equipped with the dual norm. Then, by multiplying (1.3), (1.8) and (1.9) with adequate test functions, applying Green's formula, using the interface conditions (1.10) and (1.11), the boundary conditions (1.13) and (1.14), substituting (1.12) into the first term of (1.9), and assuming sufficiently smooth data, we obtain the variational formulation: Find $p \in H^1(0,T;L^2(\Omega)) \cap L^\infty(0,T;Q)$, $\boldsymbol{u} \in H^1(0,T;V)$, and $\tilde{q}_L \in L^2(0,T;H^1_w(\mathscr{C})')$ solution a.e. in $]0,T[$ of:

$$2G(\boldsymbol{\varepsilon}(\boldsymbol{u}), \boldsymbol{\varepsilon}(\boldsymbol{v})) + \lambda(\nabla\cdot\boldsymbol{u}, \nabla\cdot\boldsymbol{v}) - \alpha(p, \nabla\cdot\boldsymbol{v}) \\ + (p_c, [\boldsymbol{v}]_\mathscr{C}\cdot\boldsymbol{n}^+)_\mathscr{C} = (\boldsymbol{f}, \boldsymbol{v}), \forall\boldsymbol{v} \in V \tag{2.7}$$

$$\forall\theta \in Q, \left(\frac{1}{M} + c_f\varphi_0\right)(p_t, \theta) + \alpha(\nabla\cdot\boldsymbol{u}_t, \theta) \\ + \frac{1}{\mu_f}(\boldsymbol{K}(\nabla p - \rho_{f,r}g\nabla\eta), \nabla\theta) = (\tilde{q}, \theta) + \langle\tilde{q}_L, \theta_c\rangle_\mathscr{C} \tag{2.8}$$

where the scalar products are taken in $\Omega\backslash\mathscr{C}$,

$$-([\boldsymbol{u}_t]_\mathscr{C}\cdot\boldsymbol{n}^+, \theta_c)_\mathscr{C} + \left(\frac{w^3}{12\mu_f}(\overline{\nabla} p_c - \rho_{f,r}g\overline{\nabla}\eta), \overline{\nabla}\theta_c\right)_\mathscr{C} \\ = \langle\tilde{q}_I - \tilde{q}_L, \theta_c\rangle_\mathscr{C}, \forall\theta \in Q \tag{2.9}$$

with the initial condition at time $t = 0$

$$p(0) = p_0 \tag{2.10}$$

2.2 Two Reduced Formulations

A first reduced formulation is obtained by summing (2.8) and (2.9), thereby eliminating $\tilde{q}_L$: Find $p \in H^1$

$(0, T; L^2(\Omega)) \cap L^2(0, T; Q)$ and $\boldsymbol{u} \in H^1(0, T; V)$, solution of (2.10) and a.e. in $]0, T[$ of (2.7) and for all $\theta \in Q$:

$$
\begin{aligned}
&\left(\tfrac{1}{M} + c_f \varphi_0\right)(p_t, \theta) + \alpha(\nabla \cdot \boldsymbol{u}_t, \theta) - ([\boldsymbol{u}_t]_{\mathscr{C}} \cdot \boldsymbol{n}^+, \theta_c)_{\mathscr{C}} \\
&\quad + \tfrac{1}{\mu_f}(\boldsymbol{K}(\nabla p - \rho_{f,r} g \nabla \eta), \nabla \theta) \\
&+ \left(\tfrac{w^3}{12\mu_f}(\overline{\nabla} p_c - \rho_{f,r} g \overline{\nabla} \eta), \overline{\nabla} \theta_c\right)_{\mathscr{C}} = (\tilde{q}, \theta) + (\tilde{q}_I, \theta_c)_{\mathscr{C}}.
\end{aligned}
\tag{2.11}
$$

Next, (2.7) can be viewed as an equation for the displacement $\boldsymbol{u}$ as an affine function of p. More precisely, we split $\boldsymbol{u}$ into two parts:

$$
\boldsymbol{u} = \bar{\boldsymbol{u}} + \boldsymbol{u}(p)
$$

where, for $\boldsymbol{f}$ given in $L^2(\Omega)^d$, $\bar{\boldsymbol{u}} \in V$ solves for all $\boldsymbol{v} \in V$:
$$
2G(\boldsymbol{\varepsilon}(\bar{\boldsymbol{u}}), \boldsymbol{\varepsilon}(\boldsymbol{v})) + \lambda(\nabla \cdot \bar{\boldsymbol{u}}, \nabla \cdot \boldsymbol{v}) = (\boldsymbol{f}, \boldsymbol{v})
\tag{2.12}
$$

and for p given in $H^1(\Omega)$, $\boldsymbol{u}(p) \in V$ solves for all $\boldsymbol{v} \in V$:

$$
\begin{aligned}
&2G(\boldsymbol{\varepsilon}(\boldsymbol{u}(p)), \ \boldsymbol{\varepsilon}(\boldsymbol{v})) + \lambda(\nabla \cdot \boldsymbol{u}(p), \nabla \cdot \boldsymbol{v}) \\
&\quad = \alpha(p, \nabla \cdot \boldsymbol{v}) - (p_c, [\boldsymbol{v}]_{\mathscr{C}} \cdot \boldsymbol{n}^+)_{\mathscr{C}}
\end{aligned}
\tag{2.13}
$$

It is easy to prove that each of these two systems has a unique solution. This leads to a second reduced problem: Find $p \in H^1(0, T; L^2(\Omega)) \cap L^2(0, T; Q)$ solution of (2.10) and:

$$
\begin{aligned}
&\forall \theta \in Q, \ \left(\tfrac{1}{M} + c_f \varphi_0\right)(p_t, \theta) + \alpha(\nabla \cdot (\bar{\boldsymbol{u}}_t + \boldsymbol{u}(p_t)), \theta) \\
&- ([\bar{\boldsymbol{u}}_t + \boldsymbol{u}(p_t)]_{\mathscr{C}} \cdot \boldsymbol{n}^+, \theta_c)_{\mathscr{C}} + \tfrac{1}{\mu_f}(\boldsymbol{K}(\nabla p - \rho_{f,r} g \nabla \eta), \nabla \theta) \\
&+ \left(\tfrac{w^3}{12\mu}(\overline{\nabla} p_c - \rho_{f,r} g \overline{\nabla} \eta), \overline{\nabla} \theta_c\right)_{\mathscr{C}} = (\tilde{q}, \theta) + (\tilde{q}_I, \theta_c)_{\mathscr{C}}
\end{aligned}
\tag{2.14}
$$

where $\bar{\boldsymbol{u}} \in H^1(0, T; V)$ and $\boldsymbol{u}(p) \in H^1(0, T; V)$ are the unique solutions of (2.12) and (2.13) respectively. The advantage of (2.14) is that its only unknown is p.

2.3 Existence and Uniqueness

The analysis of Problem (2.7-2.10) relies on suitable properties of $H_w^1(\mathscr{C})$, that in turn depend on the regularity of w. For the practical applications we have in mind, w has the following properties when $d = 3$; the statement easily extends to $d = 2$.

Hypothesis 1. *The non negative function w is H^1 in time and is smooth in space away from the crack front, i.e. the boundary $\partial \mathscr{C}$. It vanishes on $\partial \mathscr{C}$ and in a neighborhood of any point of $\partial \mathscr{C}$, w is asymptotically of the form:*

$$
w(x, y) \simeq x^{1/2} f(y)
\tag{2.15}
$$

where y is locally parallel to the crack front, x is the distance to the crack, and f is smooth.

With this hypothesis, we can validate the integrations by parts required to pass from Problem (Q) to its variational formulation (2.7-2.9) and we recover the leakoff unknown $\tilde{q}_L$ from (2.11), thus showing equivalence between all three formulations. This equivalence allows to "construct" a solution of Problem (Q) by discretizing (2.14) with a Galerkin method, more precisely by approximating p in a truncated basis, say of dimension m, of the space Q. This leads to a square system of linear Ordinary Differential Equations of order one and of dimension m, with an initial condition. A close examination of this system's matrices shows that it has a unique solution. Then reasonable regularity assumptions on the data, Hypothesis 1, and the theory developed by [18], yield a set of basic *a priori* estimates on the discrete pressure, say p_m, and displacement $\boldsymbol{u}(p_m)$. These are sufficient to pass to the limit in the discrete version of (2.14), but, as is the case of a poro-elastic system, they are not sufficient to recover the initial condition on p. This initial condition can be recovered by means of a suitable *a priori* estimate on the time derivative p'_m, but it requires a slightly stronger regularity assumption on the data (still fairly reasonable) and an assumption on the time growth of w. It allows the time evolution of a crack, but it cannot be used in the formation of a crack, since it forbids an opening of a region that is originally closed. More precisely, we make the following hypothesis.

Hypothesis 2. *There exists a constant C such that:*

$$
a.e. \ in \ \mathscr{C} \times]0, T[, \ w' \leq C w
\tag{2.16}
$$

With this additional assumption, we can prove existence and uniqueness of a solution of Problem (Q).

Theorem 1. *If $\boldsymbol{f}$ is in $H^2(0, T; L^2(\Omega)^d)$, $\tilde{q}$ in $L^2(\Omega \times]0, T[)$, $\tilde{q}_I$ in $H^1(0, T; L^2(\mathscr{C}))$, p_0 in Q, and w satisfies Hypotheseses 1 and 2, then the linearized problem (2.7-2.10) has one and only one solution p in $H^1(0, T; L^2(\Omega)) \cap L^2(0, T; Q)$, $\boldsymbol{u}$ in $H^1(0, T; V)$, and $\tilde{q}_L$ in $L^2(0, T; H_w^1(\mathscr{C})')$. This solution depends continuously on the data.*

2.4 Heuristic Mixed Formulation

A mixed formulation for the flow is useful in view of discretization because it leads to locally conservative schemes. The mixed formulation we present in this short section is derived heuristically in the sense that it is written in spaces of sufficiently smooth functions in the fracture. As the discrete functions are always locally smooth, all terms in the discrete formulation will make sense.

For the pressure in $\Omega \setminus \mathscr{C}$, we define the auxiliary velocity $\boldsymbol{z}$ by:

$$
\boldsymbol{z} = -\boldsymbol{K} \nabla(p - \rho_{f,r} g \eta)
\tag{2.17}
$$

and for the pressure in $\mathscr{C}$, we define a surface velocity ζ by:

$$\zeta = -\overline{\nabla}\left(p_c - \rho_{f,r}g\eta\right) \qquad (2.18)$$

Let:

$$\boldsymbol{Z} = \{\boldsymbol{q} \in H(\mathrm{div}; \Omega^+ \cup \Omega^-); \ [\boldsymbol{q}] \cdot \boldsymbol{n}^+ = 0 \text{ on } \Gamma\backslash\mathscr{C}$$
$$\boldsymbol{q} \cdot \boldsymbol{n} = 0 \text{ on } \partial\Omega\}$$
$$\boldsymbol{Z}_\mathscr{C} = \{\boldsymbol{\mu} \in L^2(\mathscr{C})^{d-1}; \ \overline{\nabla} \cdot (w^3\boldsymbol{\mu}) \in L^2(\mathscr{C})\}$$

In view of (1.13), (1.11), and the regularity in Theorem 1, we have $\boldsymbol{z} \in \boldsymbol{Z}$ and we see that it must satisfy the essential jump condition:

$$\frac{1}{\mu_f}[\boldsymbol{z}]_\mathscr{C} \cdot \boldsymbol{n}^+ = -\tilde{q}_L \text{ on } \mathscr{C} \qquad (2.19)$$

We use the same space V for $\boldsymbol{u}$, but we reduce the regularity of p and set:

$$Q = L^2(\Omega)$$

As the trace of functions in Q are no longer meaningful, we introduce an additional variable p_c in the space:

$$\Theta_\mathscr{C} = L^2(\mathscr{C})$$

and we assume that the leakoff term is in $\Theta_\mathscr{C}$. Then the mixed variational formulation reads (to simplify, we do not specify the dependence of the spaces on time): Find $\boldsymbol{u} \in V$, $p \in Q$, $p_c \in \Theta_\mathscr{C}$, $\tilde{q}_L \in \Theta_\mathscr{C}$, $\boldsymbol{z} \in \boldsymbol{Z}$, and $\zeta \in \boldsymbol{Z}_\mathscr{C}$ such that (2.7), (2.10), and (2.19) hold:

$$2G(\boldsymbol{\varepsilon}(\boldsymbol{u}), \boldsymbol{\varepsilon}(\boldsymbol{v})) + \lambda(\nabla \cdot \boldsymbol{u}, \nabla \cdot \boldsymbol{v}) - \alpha(p, \nabla \cdot \boldsymbol{v})$$
$$+(p_c, [\boldsymbol{v}]_\mathscr{C} \cdot \boldsymbol{n}^+)_\mathscr{C} = (\boldsymbol{f}, \boldsymbol{v}), \ \forall \boldsymbol{v} \in V$$

$$p(0) = p_0$$

$$\frac{1}{\mu_f}[\boldsymbol{z}]_\mathscr{C} \cdot \boldsymbol{n}^+ = -\tilde{q}_L \text{ on } \mathscr{C}$$

and for all θ in Q:

$$\left(\frac{1}{M} + c_f\varphi_0\right)(p_t, \theta) + \alpha(\nabla \cdot \boldsymbol{u}_t, \theta) + \frac{1}{\mu_f}(\mathrm{div}\,\boldsymbol{z}, \theta) = (\tilde{q}, \theta) \qquad (2.20)$$

for all θ_c in $\Theta_\mathscr{C}$

$$-([\boldsymbol{u}_t]_\mathscr{C} \cdot \boldsymbol{n}^+, \theta_c)_\mathscr{C} + \frac{1}{12\mu_f}(\overline{\nabla} \cdot (w^3\zeta), \theta_c)_\mathscr{C} = (\tilde{q}_I - \tilde{q}_L, \theta_c)_\mathscr{C} \qquad (2.21)$$

$$\forall \boldsymbol{q} \in \boldsymbol{Z}, \ (\boldsymbol{K}^{-1}\boldsymbol{z}, \boldsymbol{q}) = (p, \nabla \cdot \boldsymbol{q}) - (p_c, [\boldsymbol{q}]_\mathscr{C} \cdot \boldsymbol{n}^+)_\mathscr{C}$$
$$+ (\overline{\nabla}(\rho_{f,r}g\eta), \boldsymbol{q}) \qquad (2.22)$$

$$\forall \boldsymbol{\mu} \in \boldsymbol{Z}_\mathscr{C}, \ (w^3\zeta, \boldsymbol{\mu})_\mathscr{C} = (p_c, \overline{\nabla} \cdot (w^3\boldsymbol{\mu}))_\mathscr{C}$$
$$+ (\overline{\nabla}(\rho_{f,r}g\eta), w^3\boldsymbol{\mu})_\mathscr{C} \qquad (2.23)$$

It follows from (2.22) that p belongs to $H^1(\Omega)$ and $p_c = p|_\mathscr{C}$. Hence p_c acts like a Lagrange multiplier that enforces the continuity of the traces on $\mathscr{C}$. Moreover, when the solutions are sufficiently smooth, the mixed and primitive formulations are equivalent. In addition, $\tilde{q}_L$ can be immediately eliminated by substituting (2.19) into (2.21); this yields:

$$\forall \theta_c \in \Theta_\mathscr{C}, \ -([\boldsymbol{u}_t]_\mathscr{C} \cdot \boldsymbol{n}^+, \theta_c)_\mathscr{C} + \frac{1}{12\mu_f}(\overline{\nabla} \cdot (w^3\zeta), \theta_c)_\mathscr{C}$$
$$- \frac{1}{\mu_f}([\boldsymbol{z}]_\mathscr{C} \cdot \boldsymbol{n}^+, \theta_c)_\mathscr{C} = (\tilde{q}_I, \theta_c)_\mathscr{C} \qquad (2.24)$$

3 DISCRETIZATION

In this section, we present a space-time discretization of the linearized problem (2.7), (2.10), (2.20), (2.22), (2.23), (2.24) with a backward Euler scheme in time and Galerkin finite elements in space for the displacement, except in a neighborhood of the crack. The flow equation is discretized by a Multipoint Flux Mixed Finite Element Method (MFMFE). In order to avoid handling curved elements or approximating curved surfaces, we assume that both $\partial\Omega$ and the crack $\mathscr{C}$ are polygonal or polyhedral surfaces. We shall refer to this scheme as the MFMFE-CG scheme. A convergence analysis of the MFE-CG scheme for the poro-elasticity system without a crack is done in [17], where two versions of the method: one with a symmetric quadrature rule on simplicial grids or on smooth quadrilateral and hexahedral grids, and one with a non-symmetric quadrature rule on rough quadrilateral and hexahedral grids are treated. Theoretical and numerical results demonstrated first order convergence in time and space for the fluid pressure and velocity as well as for solid displacement. In the formulation below, we restrict our attention to the symmetric quadrature rule for the flow.

3.1 MFMFE Spaces

We first describe the interior discretization. Let $\overline{\Omega}$ be exactly partitioned into a conforming union of finite elements of characteristic size h, i.e. without hanging nodes. For convenience we assume that the elements are

quadrilaterals in 2D and hexahedra in 3D. Let us denote the partition by $\mathscr{T}_h$ and assume that it is shape-regular [20]. For convenience, we also assume that $\mathscr{T}_h$ triangulates exactly Ω^+ and Ω^-; in particular, no element crosses $\mathscr{C}$. The displacement, velocity and pressure finite element spaces on any physical element E are defined, respectively, *via* the vector transformation:

$$\boldsymbol{v} \leftrightarrow \hat{\boldsymbol{v}} : \boldsymbol{v} = \hat{\boldsymbol{v}} \circ F_E^{-1}$$

via the Piola transformation:

$$\boldsymbol{z} \leftrightarrow \hat{\boldsymbol{z}} : \boldsymbol{z} = \frac{1}{J_E} \mathbb{D}\mathbb{F}_E \hat{\boldsymbol{z}} \circ F_E^{-1} \qquad (3.1)$$

and *via* the scalar transformation:

$$w \leftrightarrow \hat{w} : w = \hat{w} \circ F_E^{-1}$$

where F_E denotes a mapping from the reference element $\hat{E}$ to the physical element E, $\mathbb{D}\mathbb{F}_E$ is the Jacobian of F_E, and J_E is its determinant. The advantage of the Piola transformation is that it preserves the divergence and the normal components of the velocity vectors on the faces (edges) [21, see Chap.III, 4.4], [22]:

$$(\nabla \cdot \boldsymbol{v}, w)_E = (\hat{\nabla} \cdot \hat{\boldsymbol{v}}, \hat{w})_{\hat{E}} \text{ and } (\boldsymbol{v} \cdot \boldsymbol{n}_e, w)_e = (\hat{\boldsymbol{v}} \cdot \hat{\boldsymbol{n}}_{\hat{e}}, \hat{w})_{\hat{e}} \qquad (3.2)$$

which is needed for an $H(\text{div}; \Omega)$-conforming velocity space as required by (3.3).

The finite element spaces V_h, Z_h and Q_h on $\mathscr{T}_h$ are given by:

$$
\begin{aligned}
\boldsymbol{V}_h &= \left\{ \boldsymbol{v} \in \boldsymbol{V}; \boldsymbol{v}|_E \leftrightarrow \hat{\boldsymbol{v}}, \hat{\boldsymbol{v}} \in \hat{\boldsymbol{V}}(\hat{E}), \forall E \in \mathscr{T}_h \right\} \\
\boldsymbol{Z}_h &= \left\{ \boldsymbol{z} \in \boldsymbol{Z}; \boldsymbol{z}|_E \leftrightarrow \hat{\boldsymbol{z}}, \hat{\boldsymbol{z}} \in \hat{\boldsymbol{Z}}(\hat{E}), \forall E \in \mathscr{T}_h \right\} \quad (3.3)\\
Q_h &= \left\{ q \in Q; q|_E \leftrightarrow \hat{q}, \hat{q} \in \hat{Q}(\hat{E}), \forall E \in \mathscr{T}_h \right\}
\end{aligned}
$$

where $\hat{\boldsymbol{V}}(\hat{E})$, $\hat{\boldsymbol{Z}}(\hat{E})$ and $\hat{Q}(\hat{E})$ are finite element spaces on the reference element $\hat{E}$. Note that since $\mathscr{C}$ is an open set and V_h is contained in V, the functions of V_h are continuous on $\partial\mathscr{C}$, *i.e.* they have no jump on $\partial\mathscr{C}$.

Let P_k denote the space of polynomials of degree k in two or three variables, and let Q_1 denote the bilinear or trilinear polynomial spaces in two or three variables, according to the dimension.

Convex Quadrilaterals

In the case of convex quadrilaterals, $\hat{E}$ is the unit square with vertices $\hat{\boldsymbol{r}}_1 = (0,0)^T$, $\hat{\boldsymbol{r}}_2 = (1,0)^T$, $\hat{\boldsymbol{r}}_3 = (1,1)^T$, and $\hat{\boldsymbol{r}}_4 = (0,1)^T$. Denote by $\boldsymbol{r}_i, i = 1, \ldots, 4$ the corresponding

vertices of E. In this case, F_E is the bilinear mapping given as:

$$
\begin{aligned}
F_E(\hat{x}, \hat{y}) = &\, \boldsymbol{r}_1(1-\hat{x})(1-\hat{y}) + \boldsymbol{r}_2\hat{x}(1-\hat{y}) + \boldsymbol{r}_3\hat{x}\hat{y} \\
&+ \boldsymbol{r}_4(1-\hat{x})\hat{y}
\end{aligned}
$$

the space for the displacement is:

$$\hat{\boldsymbol{V}}(\hat{E}) = Q_1(\hat{E})^2$$

and the space for the flow is the lowest order BDM_1 [23] space:

$$\hat{\boldsymbol{Z}}(\hat{E}) = P_1(\hat{E})^2 + r\,\text{curl}(\hat{x}^2\hat{y}) + s\,\text{curl}(\hat{x}\hat{y}^2)$$

$$\hat{Q}(\hat{E}) = P_0(\hat{E})$$

where r and s are real constants.

Hexahedra

In the case of hexahedra, $\hat{E}$ is the unit cube with vertices $\hat{\boldsymbol{r}}_1 = (0,0,0)^T$, $\hat{\boldsymbol{r}}_2 = (1,0,0)^T$, $\hat{\boldsymbol{r}}_3 = (1,1,0)^T$, $\hat{\boldsymbol{r}}_4 = (0,1,0)^T$, $\hat{\boldsymbol{r}}_5 = (0,0,1)^T$, $\hat{\boldsymbol{r}}_6 = (1,0,1)^T$, $\hat{\boldsymbol{r}}_7 = (1,1,1)^T$, and $\hat{\boldsymbol{r}}_8 = (0,1,1)^T$. Denote by $\boldsymbol{r}_i = (x_i, y_i, z_i)^T, i = 1, \ldots, 8$, the eight corresponding vertices of E. We note that the element can have non-planar faces. In this case F_E is a trilinear mapping given by:

$$
\begin{aligned}
F_E(\hat{x}, \hat{y}, \hat{z}) = &\, \boldsymbol{r}_1(1-\hat{x})(1-\hat{y})(1-\hat{z}) + \boldsymbol{r}_2\hat{x}(1-\hat{y})(1-\hat{z}) \\
&+ \boldsymbol{r}_3\hat{x}\hat{y}(1-\hat{z}) + \boldsymbol{r}_4(1-\hat{x})\hat{y}(1-\hat{z}) + \boldsymbol{r}_5(1-\hat{x})(1-\hat{y})\hat{z} \\
&+ \boldsymbol{r}_6\hat{x}(1-\hat{y})\hat{z} + \boldsymbol{r}_7\hat{x}\hat{y}\hat{z} + \boldsymbol{r}_8(1-\hat{x})\hat{y}\hat{z}
\end{aligned}
$$

and the spaces are defined by:

$$\hat{\boldsymbol{V}}(\hat{E}) = Q_1(\hat{E})^3$$

for the displacement, and by enhancing the BDDF_1 spaces [14] for the flow:

$$
\begin{aligned}
\hat{\boldsymbol{Z}}(\hat{E}) = &\, \text{BDDF}_1(\hat{E}) \\
&+ s_2\textbf{curl}(0,0,\hat{x}^2\hat{z})^T + s_3\textbf{curl}(0,0,\hat{x}^2\hat{y}\hat{z})^T \\
&+ t_2\textbf{curl}(\hat{x}\hat{y}^2,0,0)^T + t_3\textbf{curl}(\hat{x}\hat{y}^2\hat{z},0,0)^T \qquad (3.4)\\
&+ w_2\textbf{curl}(0,\hat{y}\hat{z}^2,0)^T + w_3\textbf{curl}(0,\hat{x}\hat{y}\hat{z}^2,0)^T \\
\hat{Q}(\hat{E}) = &\, P_0(\hat{E})
\end{aligned}
$$

where the $\text{BDDF}_1(\hat{E})$ space is defined as [24]:

$$
\begin{aligned}
\text{BDDF}_1(\hat{E}) = &\, P_1(\hat{E})^3 + s_0\textbf{curl}(0,0,\hat{x}\hat{y}\hat{z})^T \\
&+ s_1\textbf{curl}(0,0,\hat{x}\hat{y}^2)^T + t_0\textbf{curl}(\hat{x}\hat{y}\hat{z},0,0)^T \\
&+ t_1\textbf{curl}(\hat{y}\hat{z}^2,0,0)^T + w_0\textbf{curl}(0,\hat{x}\hat{y}\hat{z},0)^T \\
&+ w_1\textbf{curl}(0,\hat{x}^2\hat{z},0)^T
\end{aligned}
$$

In the above equations, s_i, t_i, w_i $(i = 0, \ldots, 3)$ are real constants. In all cases, the Degrees of Freedom (DOF) for the displacements are chosen as Lagrangian nodal point values. The velocity DOF are chosen to be the normal components at the d vertices on each face. The dimension of the space is dn_v, where d is the dimension and n_v is the number of vertices in E. Note that, although the original BDDF$_1$ spaces have only three DOF on square faces, these spaces have been enhanced in [14] to have four DOF on square faces. This special choice is needed in the reduction to a cell-centered pressure stencil in a pure Darcy flow problem as described later in this section.

3.2 A Quadrature Rule

The integration on a physical element is performed by mapping to the reference element and choosing a quadrature rule on $\hat{E}$. Using the Piola transformation, we write $(\boldsymbol{K}^{-1}\cdot, \cdot)$ in (2.22) as:

$$(\boldsymbol{K}^{-1}\boldsymbol{z}, \boldsymbol{q})_E = \left(\frac{1}{J_E}\mathbb{D}\mathbb{F}_E^T\boldsymbol{K}^{-1}(F_E(\hat{\boldsymbol{x}}))\mathbb{D}\mathbb{F}_E\hat{\boldsymbol{z}}, \hat{\boldsymbol{q}}\right)_{\hat{E}}$$

$$\equiv (\mathscr{M}_E\hat{\boldsymbol{z}}, \hat{\boldsymbol{q}})_{\hat{E}}$$

where:

$$\mathscr{M}_E = \frac{1}{J_E}\mathbb{D}\mathbb{F}_E^T\boldsymbol{K}^{-1}(F_E(\hat{\boldsymbol{x}}))\mathbb{D}\mathbb{F}_E \qquad (3.5)$$

Then, we denote the trapezoidal rule on $\hat{E}$ by $\text{Trap}(\cdot, \cdot)_{\hat{E}}$:

$$\text{Trap}(\hat{\boldsymbol{z}}, \hat{\boldsymbol{q}})_{\hat{E}} \equiv \frac{|\hat{E}|}{k}\sum_{i=1}^{k}\hat{\boldsymbol{z}}(\hat{\boldsymbol{r}}_i) \cdot \hat{\boldsymbol{q}}(\hat{\boldsymbol{r}}_i) \qquad (3.6)$$

where $\{\hat{\boldsymbol{r}}_i\}_{i=1}^{k}$ are the vertices of $\hat{E}$. The quadrature rule on an element E is defined as:

$$(\boldsymbol{K}^{-1}\boldsymbol{z}, \boldsymbol{q})_{Q,E} \equiv \text{Trap}(\mathscr{M}_E\hat{\boldsymbol{z}}, \hat{\boldsymbol{q}})_{\hat{E}}$$
$$= \frac{|\hat{E}|}{k}\sum_{i=1}^{k}\mathscr{M}_E(\hat{\boldsymbol{r}}_i)\hat{\boldsymbol{z}}(\hat{\boldsymbol{r}}_i) \cdot \hat{\boldsymbol{q}}(\hat{\boldsymbol{r}}_i) \qquad (3.7)$$

Mapping back to the physical element E, we have the quadrature rule on E as:

$$(\boldsymbol{K}^{-1}\boldsymbol{z}, \boldsymbol{q})_{Q,E} = \frac{|\hat{E}|}{k}\sum_{i=1}^{k}J_E(\hat{\boldsymbol{r}}_i)\boldsymbol{K}^{-1}(\boldsymbol{r}_i)\boldsymbol{z}(\boldsymbol{r}_i) \cdot \boldsymbol{q}(\boldsymbol{r}_i) \qquad (3.8)$$

and we define $(\boldsymbol{K}^{-1}\boldsymbol{z}, \boldsymbol{q})_Q$ by summing (3.8) on all elements E of $\mathscr{T}_h$. As the trapezoidal rule induces a scalar

product on the above finite element spaces that yields a norm uniformly equivalent to the L^2 norm [14, 15], and the tensor $\boldsymbol{K}$ is symmetric, bounded, and uniformly positive definite, this quadrature rule also yields a norm on these spaces uniformly equivalent to the L^2 norm.

3.3. Discretization in the Fracture

Since $\mathscr{C}$ is assumed to be polygonal or polyhedral, we can map each line segment or plane face of $\mathscr{C}$ onto a segment in the x_1 line (when $d = 2$) or a polygon in the $x_1 - x_2$ plane (when $d = 3$) by a rigid-body motion that preserves both surface gradient and divergence, maps the normal $\boldsymbol{n}^+$ into a unit vector along x_3, for exemple $-\boldsymbol{e}_3$, and whose Jacobian is one. After this change in variable, all operations on this line segment or plane face can be treated as the same operations on the x_1 axis or $x_1 - x_2$ plane. To simplify, we do not use a particular notation for this change in variable, and work as if the line segments or plane faces of $\mathscr{C}$ lie on the x_1 line or $x_1 - x_2$ plane. Let $\mathscr{S}_i$, $1 \le i \le I$, denote the line segments or plane faces of $\mathscr{C}$; to simplify, we drop the index i. Let $\mathscr{T}_{\mathscr{S},h}$ be a shape regular partition of $\mathscr{S}$, for instance the trace of $\mathscr{T}_h$ on $\mathscr{S}$ (but it can be something else) let e denote a generic element of $\mathscr{T}_{\mathscr{S},h}$, with reference element $\hat{e}$, and let the scalar and Piola transforms be defined by the same formula as above, but with respect to e instead of E. Then we define the finite element spaces on $\mathscr{C}$ by:

$$\boldsymbol{Z}_{\mathscr{C},h} = \left\{\boldsymbol{z} \in \boldsymbol{Z}_{\mathscr{C}}; \boldsymbol{z}|_{\mathscr{S}_i} \in \boldsymbol{Z}_{\mathscr{S}_i,h}, 1 \le i \le I\right\}$$

$$\Theta_{\mathscr{C},h} = \left\{q \in \Theta_{\mathscr{C}}; q|_{\mathscr{S}_i} \in \Theta_{\mathscr{S}_i,h}, 1 \le i \le I\right\}$$

with:

$$\boldsymbol{Z}_{\mathscr{S},h} = \left\{\boldsymbol{z} \in \boldsymbol{Z}_{\mathscr{C}}; \boldsymbol{z}|_e \leftrightarrow \hat{\boldsymbol{z}}, \hat{\boldsymbol{z}} \in \hat{\boldsymbol{Z}}_{\mathscr{C}}(\hat{e}), \forall e \in \mathscr{T}_{\mathscr{S},h}\right\}$$

$$\Theta_{\mathscr{S},h} = \left\{q \in \Theta_{\mathscr{C}}; q|_e \leftrightarrow \hat{q}, \hat{q} \in \hat{\Theta}_{\mathscr{C}}(\hat{e}), \forall e \in \mathscr{T}_{\mathscr{S},h}\right\}$$

where $\hat{\boldsymbol{Z}}_{\mathscr{C}}(\hat{e})$ and $\hat{\Theta}_{\mathscr{C}}(\hat{e})$ are finite element spaces on the reference element $\hat{e}$.

We approximate $(w^3\boldsymbol{\zeta}, \boldsymbol{\mu})_{\mathscr{S}}$ in (2.23) by first writing:

$$(w^3\boldsymbol{\zeta}, \boldsymbol{\mu})_e = \left(\frac{1}{J_e}w(F_e(\hat{\boldsymbol{x}}))^3\mathbb{D}\mathbb{F}_e^T\mathbb{D}\mathbb{F}_e\hat{\boldsymbol{\zeta}}, \hat{\boldsymbol{\mu}}\right)_{\hat{e}} \equiv (\mathscr{M}_e\hat{\boldsymbol{\zeta}}, \hat{\boldsymbol{\mu}})_{\hat{e}}$$

where:

$$\mathscr{M}_e = \frac{1}{J_e}w(F_e(\hat{\boldsymbol{x}}))^3\mathbb{D}\mathbb{F}_e^T\mathbb{D}\mathbb{F}_e \qquad (3.9)$$

and next applying the trapezoidal rule $\text{Trap}(\cdot, \cdot)_{\hat{e}}$ on $\hat{e}$:

$$\text{Trap}(\hat{\boldsymbol{\zeta}}, \hat{\boldsymbol{\mu}})_{\hat{e}} \equiv \frac{|\hat{e}|}{k} \sum_{i=1}^{k} \hat{\boldsymbol{\zeta}}(\hat{\boldsymbol{r}}_i) \cdot \hat{\boldsymbol{\mu}}(\hat{\boldsymbol{r}}_i) \qquad (3.10)$$

where $\{\hat{\boldsymbol{r}}_i\}_{i=1}^{k}$ are the vertices of $\hat{e}$. Hence mapping back to the physical element e, we approximate $(w^3\boldsymbol{\zeta}, \boldsymbol{\mu})_e$ by:

$$(w^3\boldsymbol{\zeta}, \boldsymbol{\mu})_{Q,e} = \frac{|\hat{e}|}{k} \sum_{i=1}^{k} J_e(\hat{\boldsymbol{r}}_i) w(\boldsymbol{r}_i)^3 \boldsymbol{\zeta}(\boldsymbol{r}_i) \cdot \boldsymbol{\mu}(\boldsymbol{r}_i) \qquad (3.11)$$

and we obtain the approximation $(w^3\boldsymbol{\zeta}, \boldsymbol{\mu})_Q$ by summing over all elements of $\mathcal{T}_{\mathcal{S},h}$ and over all $\mathcal{S}$ of $\mathcal{C}$.

Let I_h denote the standard nodal Lagrange interpolant on P_1 or Q_1. Then:

$$(w^3\boldsymbol{\zeta}, \boldsymbol{\mu})_Q = (I_h(w^3)\boldsymbol{\zeta}, \boldsymbol{\mu})_Q$$

and the properties of the quadrature formula imply that:

$$\forall \mu \in \boldsymbol{Z}_{\mathcal{S},h}, \; (w^3\boldsymbol{\mu}, \boldsymbol{\mu})_Q^{\frac{1}{2}} \simeq \|I_h(w^{\frac{3}{2}})\boldsymbol{\mu}\|_{L^2(\mathcal{C})}$$

3.4 The Scheme

Let $N \geq 1$ be a fixed integer, $\Delta t = T/N$ the time step, and $t_i = i\Delta t$, $0 \leq i \leq N$, the discrete time points. We define the approximations $\boldsymbol{f}^n$ of $\boldsymbol{f}(t_n)$ and $\tilde{q}^n$ of $\tilde{q}(t_n)$ for almost every $\boldsymbol{x} \in \Omega^+ \cup \Omega^-$ or Ω by:

$$\boldsymbol{f}^n(\boldsymbol{x}) = \frac{1}{\Delta t} \int_{t_{n-1}}^{t_n} \boldsymbol{f}(\boldsymbol{x}, t) dt, \; \tilde{q}^n(\boldsymbol{x}) = \frac{1}{\Delta t} \int_{t_{n-1}}^{t_n} \tilde{q}(\boldsymbol{x}, t) dt$$
$$(3.12)$$

Similarly, we define the approximation $\tilde{q}_I^n$ of $\tilde{q}_I(t_n)$ for almost every $s \in \mathcal{C}$ by:

$$\tilde{q}_I^n(s) = \frac{1}{\Delta t} \int_{t_{n-1}}^{t_n} \tilde{q}_I(s, t) dt \qquad (3.13)$$

On the other hand, we use point values for w in time, i.e. define:

$$\forall s \in \mathcal{C}, \; w^n(s) = w(s, t_n)$$

Then we propose an iterative algorithm for solving the fully discrete version of (2.7), (2.10), (2.20), (2.22), (2.23), (2.24) that uses the quadrature rule of Sections 3.2 and 3.3. A flowchart of the scheme is given in Figure 1. It uses the Fixed Stress split iterative algorithm of Mikelić and Wheeler [25]. The mean stress is given by $\bar{\boldsymbol{\sigma}} = \frac{1}{3} \sum_{i=1}^{3} \sigma_{ii}^{\text{por}}$, where $\boldsymbol{\sigma}^{\text{por}}$ is defined by (1.1). Thus the discrete mean stress reads:

$$\bar{\boldsymbol{\sigma}}_h = \frac{\alpha^2}{c_r} \nabla \cdot \boldsymbol{u}_h - \alpha p_h$$

where:

$$c_r = \frac{3\alpha^2}{3\lambda + 2G}$$

For a given displacement and mean stress, the algorithm decouples sequentially the computation of the flow in the reservoir from that in the fracture.

Recall that the given initial pressure p_0 is sufficiently smooth and has a trace, say p_c^0, on $\mathcal{C}$; this is the initial pressure in $\mathcal{C}$.

– At time $t = 0$, let $p_h^0 = P_h(p_0)$ and $p_{c,h}^0 = \bar{P}_h(p_c^0)$ where P_h and $\bar{P}_h$ are suitable approximation operators from Q into Q_h and $\Theta_{\mathcal{C}}$ into $\Theta_{\mathcal{C},h}$ respectively. Then the initial displacement is approximated by discretizing the elasticity equation (2.13) in $\Omega \backslash \mathcal{C}$: Find $\boldsymbol{u}_h^0 \in \boldsymbol{V}_h$ solution for all $\boldsymbol{v}_h \in \boldsymbol{V}_h$ of:

$$2G(\boldsymbol{\varepsilon}(\boldsymbol{u}_h^0), \boldsymbol{\varepsilon}(\boldsymbol{v}_h)) + \lambda(\nabla \cdot \boldsymbol{u}_h^0, \nabla \cdot \boldsymbol{v}_h)$$
$$= \alpha(p_h^0, \nabla \cdot \boldsymbol{v}_h) - (p_{c,h}^0, [\boldsymbol{v}_h]_{\mathcal{C}} \cdot \boldsymbol{n}^+)_{\mathcal{C}} + (\boldsymbol{f}^0, \boldsymbol{v}_h) \qquad (3.14)$$

This gives the initial mean stress:

$$\bar{\boldsymbol{\sigma}}_h^0 = \frac{\alpha^2}{c_r} \nabla \cdot \boldsymbol{u}_h^0 - \alpha p_h^0$$

– *Marching in time.* For any n, $0 \leq n \leq N - 1$, knowing $\boldsymbol{u}_h^n$, p_h^n, $\bar{\boldsymbol{\sigma}}_h^n$ and $p_{c,h}^n$, the discrete functions at time t_{n+1} are computed iteratively by two nested loops:

– *Starting functions:*

$$p_h^{n+1,0} = p_h^n, \; \boldsymbol{u}_h^{n+1,0} = \boldsymbol{u}_h^n, \; p_{c,h}^{n+1,0} = p_{c,h}^n, \; \bar{\boldsymbol{\sigma}}_h^{n+1,0} = \bar{\boldsymbol{\sigma}}_h^n$$

– *Outer loop.* For $\ell = 0, 1, \ldots$, knowing $\boldsymbol{u}_h^{n+1,\ell}$, $\bar{\boldsymbol{\sigma}}_h^{n+1,\ell}$, and $p_{c,h}^{n+1,\ell}$ compute iteratively intermediate functions $p_h^{n+1,j}$, $\boldsymbol{z}_h^{n+1,j}$, $\boldsymbol{\zeta}_h^{n+1,j}$, and $p_{c,h}^{n+1,j}$, for $j = 1, 2, \ldots, j_m$ by the inner loop written below. Set:

$$p_h^{n+1,\ell+1} := p_h^{n+1,j_m}, \; p_{c,h}^{n+1,\ell+1} := p_{c,h}^{n+1,j_m}$$

and compute the displacement $\boldsymbol{u}_h^{n+1,\ell+1} \in \boldsymbol{V}_h$ by solving for all $\boldsymbol{v}_h \in \boldsymbol{V}_h$:

$$2G(\boldsymbol{\varepsilon}(\boldsymbol{u}_h^{n+1,\ell+1}), \boldsymbol{\varepsilon}(\boldsymbol{v}_h)) + \lambda(\nabla \cdot \boldsymbol{u}_h^{n+1,\ell+1}, \nabla \cdot \boldsymbol{v}_h)$$
$$= \alpha(p_h^{n+1,\ell+1}, \nabla \cdot \boldsymbol{v}_h) - (p_{c,h}^{n+1,\ell+1}, [\boldsymbol{v}_h]_{\mathcal{C}} \cdot \boldsymbol{n}^+)_{\mathcal{C}}$$
$$+ (\boldsymbol{f}^{n+1}, \boldsymbol{v}_h)$$
$$(3.15)$$

Update the mean stress by:

$$\bar{\sigma}_h^{n+1,\ell+1} = \frac{\alpha^2}{c_r} \nabla \cdot \boldsymbol{u}_h^{n+1,\ell+1} - \alpha p_h^{n+1,\ell+1}$$

and test the difference in porosities (see Eq. 1.5):

$$\alpha \nabla \cdot \left(\boldsymbol{u}_h^{n+1,\ell+1} - \boldsymbol{u}_h^{n+1,\ell} \right) + \frac{1}{M} \left(p_h^{n+1,\ell+1} - p_h^{n+1,\ell} \right)$$

If it is larger than the tolerance, increment ℓ and return to the outer loop. Otherwise, set:

$$\boldsymbol{u}_h^{n+1} := \boldsymbol{u}_h^{n+1,\ell+1}, \; p_h^{n+1} = p_h^{n+1,\ell+1}, \; p_{c,h}^{n+1} := p_{c,h}^{n+1,\ell+1},$$

$$\bar{\sigma}_h^{n+1} = \bar{\sigma}_h^{n+1,\ell+1}$$

increment n and return to the marching in time.
– *Inner loop*. Set:

$$p_{c,h}^{n+1,0} := p_{c,h}^{n+1,\ell}$$

– For $j = 0, 1, \ldots$, knowing $\bar{\sigma}_h^{n+1,\ell}$, $\boldsymbol{u}_h^{n+1,\ell}$, and $p_{c,h}^{n+1,j}$, compute $p_h^{n+1,j+1} \in Q_h$ and $z_h^{n+1,j+1} \in \boldsymbol{Z}_h$ solution of:

$$\left(\frac{1}{M} + c_f \varphi_0 \right) \frac{1}{\Delta t} (p_h^{n+1,j+1} - p_h^n, \theta_h) + \frac{1}{\mu_f} (\text{div}\, z_h^{n+1,j+1}, \theta_h)$$
$$= (\tilde{q}^{n+1}, \theta_h) - \frac{c_r}{\alpha} \frac{1}{\Delta t} (\bar{\sigma}_h^{n+1,\ell} - \bar{\sigma}_h^n, \theta_h), \; \forall \theta_h \in Q_h \quad (3.16)$$

$$\forall \boldsymbol{q}_h \in \boldsymbol{Z}_h, \; (\boldsymbol{K}^{-1} z_h^{n+1,j+1}, \boldsymbol{q}_h)_Q = (p_h^{n+1,j+1}, \nabla \cdot \boldsymbol{q}_h)$$
$$- (p_{c,h}^{n+1,j}, [\boldsymbol{q}_h]_{\mathscr{C}} \cdot \boldsymbol{n}^+)_{\mathscr{C}} + (\nabla(\rho_{f,r} g \eta), \boldsymbol{q}_h) \quad (3.17)$$

Compute $\zeta_h^{n+1,j+1} \in \boldsymbol{Z}_{\mathscr{C},h}$ and $p_{c,h}^{n+1,j+1} \in \Theta_{\mathscr{C},h}$ solution for all $\theta_{c,h}$ in $\Theta_{\mathscr{C},h}$ of:

$$-\frac{1}{\Delta t} ([\boldsymbol{u}_h^{n+1,\ell} - \boldsymbol{u}_h^n]_{\mathscr{C}} \cdot \boldsymbol{n}^+, \theta_{c,h})_{\mathscr{C}}$$
$$-\frac{1}{\mu_f} ([z_h^{n+1,j+1}]_{\mathscr{C}} \cdot \boldsymbol{n}^+, \theta_{c,h})_{\mathscr{C}}$$
$$+\frac{1}{12\mu_f} (\overline{\nabla} \cdot (w(t_{n+1})^3 \zeta_h^{n+1,j+1}), \theta_{c,h})_{\mathscr{C}} \quad (3.18)$$
$$+\beta(p_{c,h}^{n+1,j+1} - p_{c,h}^{n+1,j}, \theta_{c,h})_{\mathscr{C}} = (\tilde{q}_I^{n+1}, \theta_{c,h})_{\mathscr{C}}$$

$$(w(t_{n+1})^3 \zeta_h^{n+1,j+1}, \boldsymbol{\mu}_h)_Q = (p_{c,h}^{n+1,j+1}, \overline{\nabla} \cdot (w(t_{n+1})^3 \boldsymbol{\mu}_h))_{\mathscr{C}}$$
$$+ (\overline{\nabla}(\rho_{f,r} g \eta), w(t_{n+1})^3 \boldsymbol{\mu}_h)_{\mathscr{C}}, \; \forall \boldsymbol{\mu}_h \in \boldsymbol{Z}_{\mathscr{C},h} \quad (3.19)$$

where $\beta > 0$ is a stabilizing factor to be adjusted. Test the difference $p_{c,h}^{n+1,j+1} - p_{c,h}^{n+1,j}$. If it is less than the tolerance, set:

$$j_m := j + 1, \; p_h^{n+1,j_m} := p_h^{n+1,j+1}, \; p_{c,h}^{n+1,j_m} := p_{c,h}^{n+1,j+1}$$

and return to the outer loop.

For given pressures, (3.14) and (3.15) have a unique solution. It is easy to prove that (3.16-3.17) determine $p_h^{n+1,j+1}$ and $z_h^{n+1,j+1}$, and that (3.18-3.19) determine $I_h(w(t_{n+1})^{3/2}) \zeta_h^{n+1,j+1}$ and $p_{c,h}^{n+1,j+1}$, owing in particular to the stabilizing term with factor β. Two remarks are in order regarding the algorithm. Equation (3.15) utilizes discontinuous spaces of functions on $\mathscr{C}$ and weakly imposes a traction boundary condition: $p_{c,h}^{n+1,\ell+1}$. Computing the solution relies on the work of Liu in [26]. The system (3.18-3.19) is solved in Section 4 below by means of a mimetic formulation [27], which is closely related to a mixed finite element method when using quadrilateral elements.

4 NUMERICAL EXPERIMENT

We provide the following numerical example as a simple illustration of the model and its predictive capability. Following the flowchart in Figure 1, we have implemented the fixed stress iterative coupling scheme with the inner iteration between reservoir flow and fracture flow into the IPARS reservoir simulation code.

The domain is taken to be the cube $\Omega = (0, 10)^3$ m, with a square fracture $\mathscr{C}$ centered on the plane $\{y = 5\}$ m of size 7.5×7.5 m. The domain is discretized into $5 \times 6 \times 5$ structured hexahedral elements. There are uniform mesh widths of 2 m in the x and z directions, and mesh widths of $\{2.475, 2.475, 0.05, 0.05, 2.475, 2.475\}$ m in the y direction.
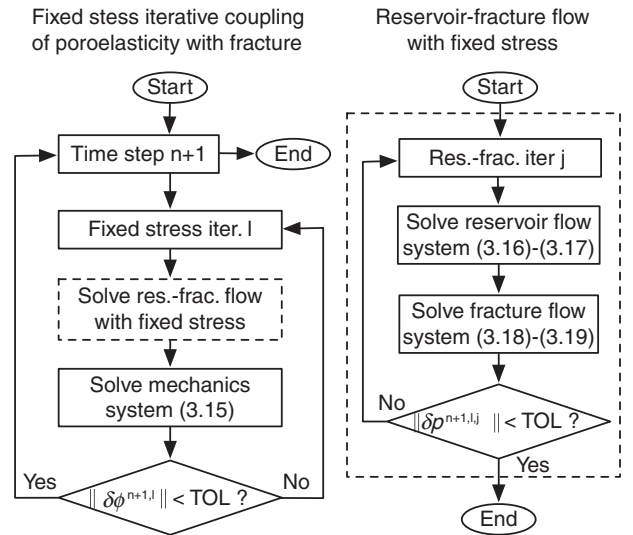

Figure 1

Flowcharts for outer iteration (left) and inner iteration (right) with fixed stress iterative coupling of poroelasticity with fracture.

TABLE 1

Input parameters for the numerical example in Si units

Parameter	Quantity	Value
K	Reservoir permeability	$diag(5, 20, 20) \times 10^{-15}$ m^2
φ^0	Initial porosity	0.2
μ	Fluid viscocity	1×10^{-3} Pa·s
c	Fluid compressibility	5.8×10^{-7} Pa^{-1}
$\rho_{f,r}$	Reference fluid density	897 kg·m^{-3}
g	Gravitational acceleration	0 m·s^{-2}
E	Young's modulus	7.0×10^{10} Pa
v	Poisson's ratio	0.3
α	Biot's coefficient	1.0
M	Biot's modulus	2.0×10^8 Pa
T	Total simulation time	20 s
Δt	Time step	1 s

The initial fluid pressure in both the reservoir and fracture is taken to be $p_0 = 3.5 \times 10^6$ Pa. The external fluid boundary conditions are set to be $p = p_0$ on $\partial\Omega$, which will allow fluid to escape as pressure rises. The external mechanical boundary conditions are such that the bottom face is completely pinned: $\boldsymbol{u} = \boldsymbol{0}$ m; the four lateral faces are traction free: $\boldsymbol{\sigma}^{por}\boldsymbol{n} = \boldsymbol{0}$ psi; and the top face has an overburden traction of $\boldsymbol{\sigma}^{por}\boldsymbol{n} = (-3.8, 0, 0) \times 10^6$ psi. The stabilization parameter is taken to be $\beta = 1.0 \times 10^{-4}$. The remaining input parameters are summarized in Table 1. The Lamé constants are given by $\lambda = Ev/[(1 + v)(1 - 2v)]$ and $G = E/[2(1 + v)]$. Fluid is injected into the center of the fracture with a constant rate of $q_I = 1\,000$ kg·s^{-1}, which will induce a pressure gradient in the fracture and leak off into the domain. Both the leak off rate q_L and the fracture pressure p_c are unknowns determined by the coupling of the reservoir and fracture flow models. The fluid pressure computed in the fracture plane is shown in Figure 2. The pressurized fracture also induces a traction on $\mathscr{C}$, which creates a discontinuity in the displacement field, allowing the calculation of a dynamic width, which is shown in Figure 3.

CONCLUSIONS

We have studied the numerical approximation of a fracture model in a poroelastic medium, where the
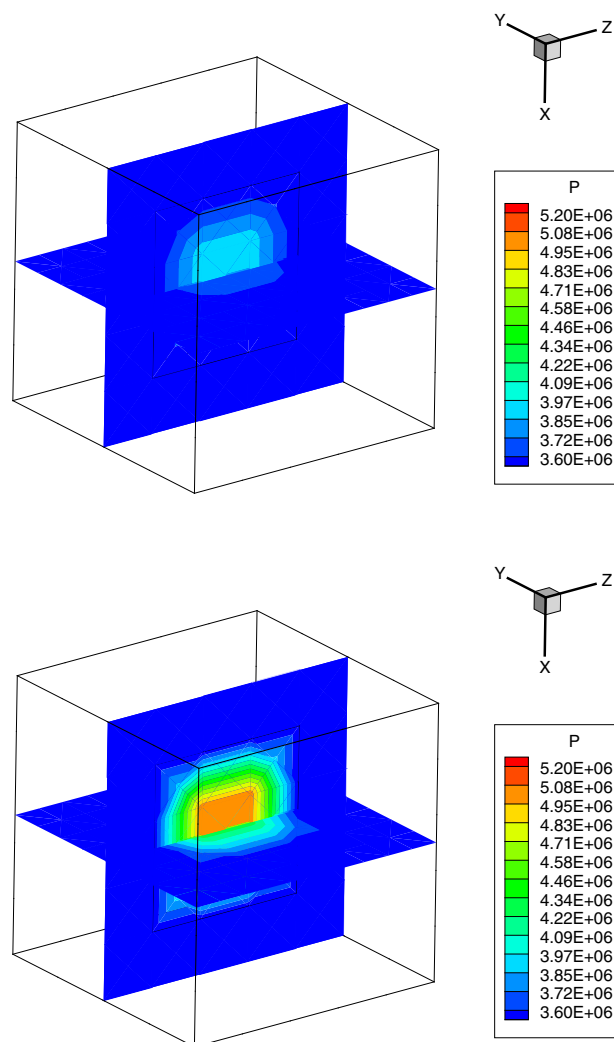

Figure 2

Computed fluid pressure in the fracture plane and a perpendicular plane on (top) the first time step, and (bottom) the final time step.

fracture is represented as a curve or surface and its width is incorporated into the flow equation in the fracture. We have used a MFMFE method for the flow in the reservoir and a Mimetic Finite Difference (MFD) method in the fracture, and a Continuous Galerkin (CG) method for the geomechanics. The scheme was solved by a fixed stress split iterative coupling for the flow and mechanics and an iterative algorithm coupling the flow in the reservoir and in the crack. A numerical experiment illustrated the relevance of the mechanical model and the efficiency of the numerical method and algorithm.
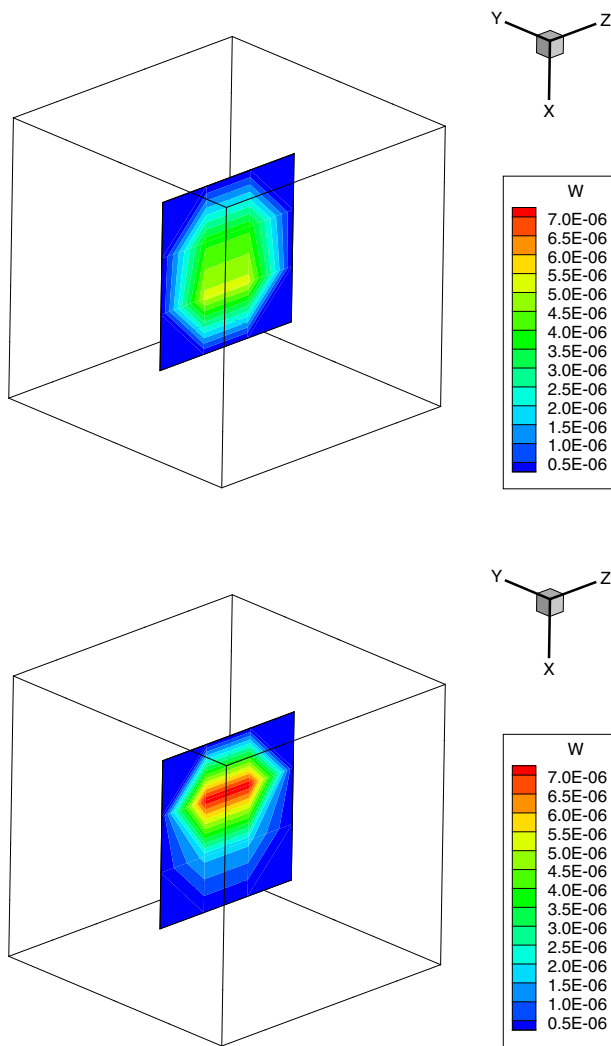
Figure 3

Computed fracture width on (top) the first time step, and (bottom) the final time step.

ACKNOWLEDGMENTS

REFERENCES

1 Dean R.H., Schmidt J.H. (2009) Hydraulic-Fracture Predictions with a Fully Coupled Geomechanical Reservoir Simulator, *SPE Journal* 707-714.

2 Chen H.Y., Teufel L.W., Lee R.L. (1995) Coupled Fluid Flow and Geomechanics in Reservoir Study – I. Theory and Governing Equations, *SPE Annual Technical Conference & Exhibition*, Dallas, Texas, Oct.

3 Morales F., Showalter R.E. (2010) The narrow fracture approximation by channeled flow, *Journal of Mathematical Analysis and Applications* **365**, 1, 320-331.

4 Morales F., Showalter R.E. (2012) Interface approximation of Darcy flow in a narrow channel, *Mathematical Methods in the Applied Sciences* **35**, 2, 182-195.

5 Alboin C., Jaffré J., Roberts J.E., Serres C. (2002) Modeling fractures as interfaces for flow and transport in porous media, Chen Z., Ewing R.E. (eds), *Fluid flow and transport in porous media: mathematical and numerical treatment, Contemporary Mathematics* **295**, 13-24, American Mathematical Society.

6 Martin V., Jaffré J., Roberts J.E. (2005) Modeling Fractures and Barriers as Interfaces for Flow in Porous Media, *SIAM J. Sci. Comput.* **26**, 5, 1667-1691.

7 Biot M.A. (1941) General Theory of Three-Dimensional Consolidation, *J. Appl. Phys.* **12**, 155-164.

8 Coussy O. (1995) *Mechanics of Porous Continua*, Wiley, New York.

9 Kim J., Tchelepi H.A., Juanes R. (2011) Stability, Accuracy, and Efficiency of Sequential Methods for Coupled Flow and Geomechanics, *SPE Journal* 249-262, June.

10 Mainguy M., Longuemare P. (2002) Coupling Fluid Flow and Rock Mechanics: Formulation of the Partial Coupling between Reservoir and Geomechanical Simulators, *Oil & Gas Science and Technology* **57**, 4, 355-367.

11 Pan F. (2009) Development and Application of a Coupled Geomechanics Model for a Parallel Compositional Reservoir Simulator, *PhD Thesis*, The University of Texas at Austin, Austin, Texas.

12 Settari A., Walters D.A. (1999) Advances in Coupled Geomechanics and Reservoir Modeling with Applications to Reservoir Compaction, *SPE Reservoir Simulation Symposium*, Houston, Texas, Feb.

13 Mikelić A., Wheeler M.F. (2013) Convergence of iterative coupling for coupled flow and geomechanics, *Computational Geosciences* **17**, 3, 455-461.

14 Ingram R., Wheeler M.F., Yotov I. (2010) A multipoint flux mixed finite element method on hexahedra, *SIAM J. Numer. Anal.* **48**, 1281-1312.

15 Wheeler M.F., Yotov I. (2006) A multipoint flux mixed finite element method, *SIAM J. Numer. Anal.* **44**, 2082-2106.

16 Wheeler M.F., Xue G., Yotov I. (2011) Accurate Cell-Centered Discretizations for Modeling Multiphase Flow in Porous Media on General Hexahedral and Simplicial Grids, *SPE Reservoir Simulation Symposium*, The Woodlands, Texas, Feb.

17 Wheeler M.F., Xue G., Yotov I. (2012) Coupling multipoint flux mixed finite element methods with continuous Galerkin methods for poroelasticity, Submitted, Aug.

18 Phillips P.J., Wheeler M.F. (2007) A Coupling of Mixed and Continuous Galerkin Finite Elements Methods for Poroelasticity I: The Continuous in Time Case, *Computational Geosciences* **11**, 131-144.

19 Rungamornrat J., Wheeler M.F., Mear M.E. (2005) Coupling of Fracture/Non-Newtonian Flow for Simulating Nonplanar Evolution of Hydraulic Fractures, *SPE Annual Technical Conference and Exhibition*, Society of Petroleum Engineers, Dallas, Texas, 9-12 Oct., *SPE Paper 96968.*

20 Ciarlet P.G. (1991) Basic error estimates for elliptic problems - Finite Element Methods, Part 1, Ciarlet P.G., Lions J.L. (eds), *Handbook of Numerical Analysis*. North-Holland, Amsterdam.

21 Girault V., Raviart P.A. (1986) *Finite element methods for Navier-Stokes equations: Theory and algorithms*, Springer Series in Computational Mathematics, 5, Springer-Verlag, Berlin.

22 Brezzi F., Fortin M. (1991) *Mixed and hybrid finite element methods*, Springer-Verlag, New York.

23 Brezzi F., Douglas J. Jr, Marini L.D. (1985) Two families of mixed elements for second order elliptic problems, *Numer. Math.* **88**, 217-235.

24 Brezzi F., Douglas J. Jr, Durán R., Fortin M. (1987) Mixed finite elements for second order elliptic problems in three variables, *Numer. Math.* **51**, 237-250.

25 Mikelić A., Bin Wang, Wheeler M.F. (2012) Numerical convergence study of iterative coupling for coupled flow and geomechanics, *ECMOR XIII - 13th European Conference on the Mathematics of Oil Recovery*, Biarritz, France, Sept.

26 Liu R. (2004) Discontinuous Galerkin for Mechanics, *PhD Thesis*, The University of Texas at Austin, Austin, Texas.

27 Berndt M., Lipnikov K., Shashkov M., Wheeler M.F., Yotov I. (2005) Superconvergence of the velocity in mimetic finite difference methods on quadrilaterals, *SIAM Journal on Numerical Analysis* **43**, 4, 1728-1749.